

SSL²: Self-Supervised Learning meets Semi-Supervised Learning: Multiple Sclerosis Segmentation in 7T-MRI from large-scale 3T-MRI

Jiacheng Wang^a, Hao Li^b, Han Liu^a, Dewei Hu^b, Daiwei Lu^a, Keejin Yoon^c, Kelsey Barter^c,
Francesca Bagnato^c, and Ipek Oguz^a

^aDept. of Computer Science, Vanderbilt University, Nashville, TN, US

^bDept. of Electrical and Computer Engineering, Vanderbilt University, Nashville, TN, US

^cDept. of Neurology, Vanderbilt University Medical Center, Nashville, TN, US

ABSTRACT

Automated segmentation of multiple sclerosis (MS) lesions from MRI scans is important to quantify disease progression. In recent years, convolutional neural networks (CNNs) have shown top performance for this task when a large amount of labeled data is available. However, the accuracy of CNNs suffers when dealing with few and/or sparsely labeled datasets. A potential solution is to leverage the information available in large public datasets in conjunction with a target dataset which only has limited labeled data. In this paper, we propose a training framework, SSL² (self-supervised-semi-supervised), for multi-modality MS lesion segmentation with limited supervision. We adopt self-supervised learning to leverage the knowledge from large public 3T datasets to tackle the limitations of a small 7T target dataset. To leverage the information from unlabeled 7T data, we also evaluate state-of-the-art semi-supervised methods for other limited annotation settings, such as small labeled training size and sparse annotations. We use the shifted-window (Swin) transformer¹ as our backbone network. The effectiveness of self-supervised and semi-supervised training strategies is evaluated in our in-house 7T MRI dataset. The results indicate that each strategy improves lesion segmentation for both limited training data size and for sparse labeling scenarios. The combined overall framework further improves the performance substantially compared to either of its components alone. Our proposed framework thus provides a promising solution for future data/label-hungry 7T MS studies.

Keywords: Self-supervised, Semi-supervised, Multiple Sclerosis, 7T MRI, Limited Supervision, Transformers

1. INTRODUCTION

Multiple Sclerosis (MS) is a prevalent inflammatory disease of the central nervous system that poses significant diagnostic and monitoring challenges. A commonly utilized tool for addressing these challenges is magnetic resonance imaging (MRI), which enables the visualization and quantification of focal MS lesions. Segmentation of these lesions is a crucial step for clinical evaluation. However, manual segmentation is time-consuming and labor-intensive, mainly due to large variations in location, shape, and intensity among lesions.

7 Tesla (7T) MRI scans provide more detailed anatomical data with higher spatial resolution and allow more precise lesion quantification. While many fully-supervised lesion segmentation algorithms²⁻⁶ exist, these are often impractical for use with 7T data, given the limited availability of publicly available annotated MS lesion datasets at 7T and the high cost of annotating in-house 7T MRI datasets.

In order to overcome the limitations posed by the scarcity of annotated data and the labor-intensive nature of manual annotation, recent research has focused on exploring self-supervised and semi-supervised learning techniques. Self-supervised learning⁷ aims to extract robust high-dimensional features directly from the MRI data using augmentations and proxy tasks. Augmentations involve transforming the data and using these transformations as supervision to learn features. Proxy tasks, such as predicting the rotation angle of an image, can then be used to train the model to learn useful features. On the other hand, semi-supervised learning leverages the abundance of unlabeled data to improve model performance.⁸ This is achieved through two main approaches: consistency learning⁹ and self-training.¹⁰ Consistency learning maximizes the stability of predictions of an unlabeled image and its noise-perturbed counterparts. Self-training generates pseudo labels from unlabeled data and retrains the model using these weak supervision signals. By utilizing both labeled and unlabeled data, semi-supervised learning offers a promising solution to the challenge of limited annotated data.

In recent years, researchers have proposed the use of transformers in the medical imaging domain to capture long-term dependencies.^{11,12} To further improve the efficiency of these approaches, the Shifted windows (Swin)-Transformer^{1,13} utilizes a non-overlapping shifted window schema to significantly reduce the computational complexity for several vision

tasks. The utilization of a Transformer-based architecture has the potential to improve the performance of MS lesion segmentation tasks by effectively capturing the long-range dependencies present in the data.

In this paper, we propose a novel approach to address the challenges of limited data and time-consuming annotations in MS lesion segmentation using MRI scans. Our approach utilizes self-supervised and semi-supervised learning methods to leverage the large number of publicly available 3T MRI scans to obtain a robust pre-trained model, using a Swin-Transformer as our backbone. We fine-tune this pre-trained model for our 7T in-house MR data on the downstream lesion segmentation task. Our hypothesis is that our pre-trained model from 3T images can boost the performance of MS lesion segmentation on a sparsely labeled 7T dataset. We consider two sparse labeling scenarios: a small number of fully labeled volumes, or volumes with only a small number of labeled slices. The contributions of our proposed self-supervised-semi-supervised learning (SSL²) framework are:

- We demonstrate a significant increase in MS lesion segmentation performance compared to traditional supervised training (Dice score improvement from 0.6971 to 0.8186) on the in-house 7T MRI dataset.
- Our proposed model generates robust segmentation results, even when using very few training samples or sparsely annotated datasets, and outperforms other methods in these limited supervision settings.
- We effectively distill knowledge from large public 3T MRI datasets to facilitate 7T MRI studies, and make the pre-trained model weights publicly available for further research *.

2. MATERIALS AND METHODS

In this section, we describe our proposed framework for addressing the challenge of limited annotation in 7T MRI scan dataset segmentation. We begin by introducing the datasets used in our framework in Section 2.1. Next, in Section 2.2, we provide an overview of the entire framework. We then delve into the key components of our framework in Sections 2.3 and 2.4, where we discuss the semi-supervised segmentation and self-supervised training, respectively. Finally, we describe our implementation details in Section 2.5.

2.1 Datasets

2.1.1 In-house 7T MRI dataset

We obtained an in-house dataset of 7T MRI scans at the Vanderbilt University Medical Center (VUMC) for 37 MS patients at various disease stages, all at their first visit. Table 1 presents the demographic and clinical information. Each subject’s data includes MP2RAGE (T1-weighted) and FLAIR scans.

Table 1. Demographic and clinical information for the VUMC 7T MS dataset.

Number of Subjects	37
Female	17 (45.9%)
Male	20 (54.1%)
Black/African American	3 (8.1%)
White/Caucasian	34 (91.9%)
RRMS (relapsing-remitting MS)	29 (78.4%)
CIS (clinically isolated syndrome)	4 (10.8%)
RIS (radiologically isolated syndrome)	2 (5.4%)
Others	2 (5.4%)
Age (mean \pm STD)	37.46 \pm 9.07
EDSS (expanded disability status scale, mean \pm STD)	1.42 \pm 1.56

Labeled 7T in-house dataset. Expert manual annotation of MS lesions on T1-weighted images was performed by a single trained annotator (KY) for a subset of 14 subjects. The automated lesion segmentation on these same 14 subjects was then performed using our existing model, ModDrop++.⁶ ModDrop++ is based on our previous Tiramisu-based model⁴ which currently holds the top position on the ISBI 2015 challenge¹⁴ leaderboard (<https://smart-stats-tools.org/lesion-challenge>). Discrepancies between the manual and automated lesion masks were reviewed and reconciled by a second trained radiologist (KB) to generate the final lesion masks for the 14 subjects.

Unlabeled 7T in-house dataset. The remaining 23 subjects are used as our unlabeled dataset.

*<https://github.com/MedICL-VU/SSL-squared-7T>

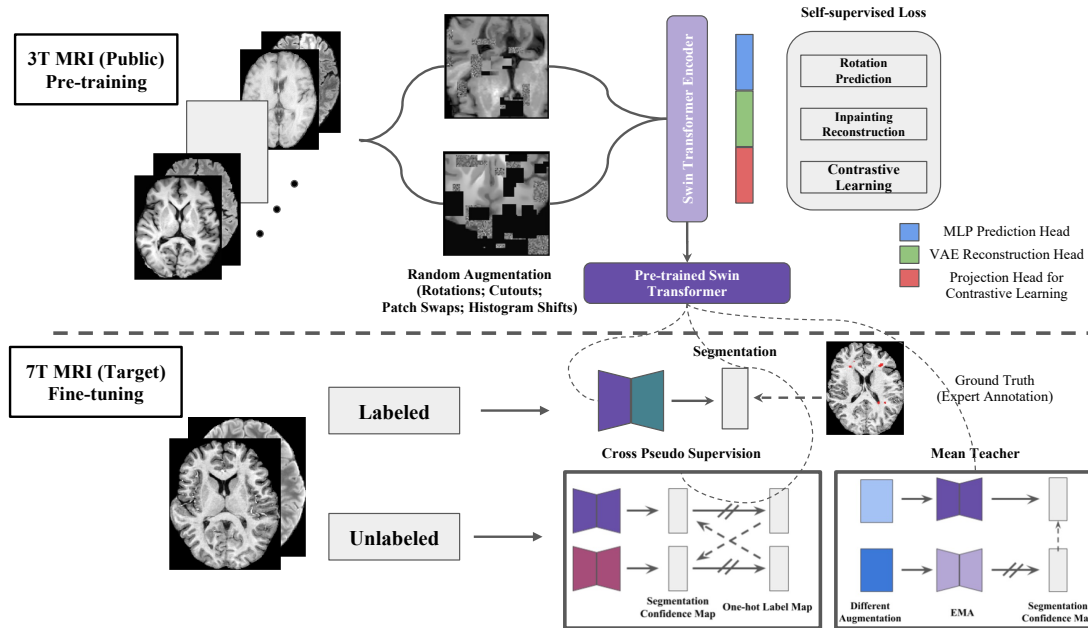


Figure 1. Overall framework. **Top.** Self-supervised pre-training. 3 heads are attached to the encoder for the 3 proxy tasks. **Bottom.** Semi-supervised fine-tuning. Pre-trained weights (purple) are used to initialize the encoder. Mean-teacher and CPS are compared.

2.1.2 Public unlabeled 3T MRI datasets

We employ several publicly available datasets without their annotations for pre-training, including:

- Longitudinal MS Lesion Segmentation Challenge (ISBI 2015) dataset,² with 21 training and 61 testing scans;
- UMCL (University Medical Center Ljubljana) Multi-rater Consensus dataset,¹⁵ with 30 scans;
- MICCAI MSSeg 2016 Challenge¹⁶ dataset, with 15 scans;
- MICCAI Brain Tumor Segmentation (BraTS) 2021 Challenge¹⁷ dataset with 1251 scans.

For consistency, only T1-weighted and FLAIR images are utilized from each of these datasets. Rigid registration is performed to align each FLAIR image to its corresponding T1w image; all T1w images are rigidly aligned to a single subject from our 7T dataset.

2.1.3 Preprocessing

We apply standard preprocessing techniques to all images (3T and 7T), including model-based skull stripping with HD-BET,¹⁸ N4 bias correction,¹⁹ and histogram normalization to the range $[0, 1]$. The resulting images have a resolution of $0.9 \times 0.9 \times 0.9\text{mm}^3$ and a field of view of $256 \times 256 \times 200$ voxels.

2.1.4 Data representation

For both the 3T and 7T MRI datasets, we crop the image to the bounding box of the skullstripped brain to reduce image size. To further address the memory constraints commonly encountered when training 3D networks, we randomly extract two sub-volumes of $96 \times 96 \times 96$ voxels from each input image. The T1w and FLAIR images are concatenated as input to our network.

2.2 System Overview

Figure 1 shows the overall workflow of our system.

We use the 7T MRI dataset (labeled and unlabeled) in a semi-supervised manner to determine the best semi-supervision strategy for the MS lesion segmentation task. We compare 6 different semi-supervised learning schemes in a 7-fold cross-validation setting. This experiment identifies the best and worst performing semi-supervision strategies, which are incorporated into our SSL^2 framework.

SSL^2 begins by using the unlabeled 3T MRI datasets to pre-train a Swin transformer model in a self-supervised manner using 3 proxy heads that correspond to 3 proxy tasks. For this purpose, we use a modification of the original 2D Swin-transformer block¹³ to be suitable for 3D volumes as our backbone network, similar to Swin-UNETR.¹³ Next, the proxy heads are discarded and only the pre-trained Swin transformer weights are preserved. The 7T MRI dataset (labeled and unlabeled) and the previously determined best-performing semi-supervision strategy are incorporated to obtain the final segmentation results. We compare this model to the baseline model which uses the worst-performing semi-supervision strategy.

2.3 Semi-supervised Segmentation in 7T MRI dataset

To choose the semi-supervision strategy for our framework, we compare the performance of six different semi-supervised learning schemes in a 7-fold cross-validation setting. These methods include Mean Teacher,⁹ Entropy Minimization,²⁰ Deep Adversarial Networks,²¹ Uncertainty Aware Mean Teacher,²² FixMatch,^{23,24} and Cross Pseudo Supervision.¹⁰

Each semi-supervised model is trained with a combination of supervised loss L_{sup} and unsupervised loss L_{unsup} such that $L_{semi} = L_{sup} + \lambda_{semi}L_{unsup}$. The supervised loss is computed using Dice Loss and pixel-wise Cross Entropy (CE) Loss, while the semi-supervised loss varies among the models. During each training iteration, equal number of labeled and unlabeled samples are used to compute L_{sup} and L_{unsup} , respectively.

Our experiments utilize the 14 subjects from our in-house 7T labeled dataset. We utilize 12 subjects for training and hold out 2 subjects for validation in each fold. Additionally, we make use of the 23 subjects in our unlabeled in-house 7T dataset for the semi-supervised models. We use a sliding-window inference method as implemented in MONAI. The window size is chosen as $96 \times 96 \times 96$ voxels with overlap of $24 \times 24 \times 24$ voxels. We use the Dice score to evaluate the performance of the compared methods.

The results are presented in Table 2. We observe that while the performance of these methods is highly comparable, the Mean Teacher⁹ performs the worst and Cross Pseudo Supervision (CPS)¹⁰ performs the best. We choose these two methods as the baseline and top performer, respectively, for the rest of our experiments. These two methods are described in more detail below.

Baseline: Mean Teacher.⁹ The Mean Teacher method utilizes two identical networks, denoted as student model $f(\theta)$ and teacher model $f(\hat{\theta})$, as shown in the left panel of Figure 2. The core idea of this method is to use the input with perturbed Gaussian noise as another input to compute the consistency loss defined as $L_{unsup} = \|P_2 - P_1\|^2$. The network parameters $f(\theta)$ are updated using $L_{semi} = L_{sup} + \lambda_{semi}L_{unsup}$ where λ_{semi} is the trade-off weight. The weights for the teacher model $f(\hat{\theta})$ are updated using the exponential moving average (EMA) to temporally ensemble the versions of the student models $f(\theta)$ from previous iterations. This strategy enforces stable predictions without the help of annotations.

Top Performer: Cross Pseudo Supervision¹⁰ (CPS). The CPS combines the ideas of self-training using pseudo labels and cross-probability consistency. It utilizes two networks, denoted $f(\theta_1)$ and $f(\theta_2)$, with different dropouts, as

Table 2. Segmentation performance (Dice score) for 6 different semi-supervised models in our 7-fold cross-validation experiment (Sec. 2.3). The fully supervised model does not have access to any unlabeled samples and thus has the lowest performance. Bold indicates the best performance in each fold. Among the semi-supervised methods, Mean Teacher is the worst performer and Cross Pseudo Supervision is the top performer for the MS lesion segmentation task.

Methods	Fold 1	Fold 2	Fold 3	Fold 4	Fold 5	Fold 6	Fold 7	Avg	Std
Fully Supervised ⁶	0.6982	0.6844	0.6867	0.6989	0.6744	0.6904	0.6964	0.6899	0.0089
Mean Teacher ⁹	0.7107	0.7048	0.6991	0.7055	0.6990	0.7088	0.7048	0.7047	0.0044
Entropy Minimization ²⁰	0.7238	0.7318	0.7312	0.7422	0.7320	0.7391	0.7257	0.7323	0.0066
Deep Adversarial Networks ⁵	0.7283	0.7455	0.7294	0.7521	0.7252	0.7263	0.7241	0.7330	0.0111
Uncertainty Aware Mean Teacher ⁹	0.7347	0.7246	0.7279	0.7351	0.7263	0.7352	0.7321	0.7308	0.0045
FixMatch ²³	0.7732	0.7753	0.7614	0.7897	0.7726	0.7656	0.7797	0.7739	0.0092
Cross Pseudo Supervision ¹⁰	0.7808	0.7894	0.7764	0.7834	0.7901	0.7803	0.7844	0.7835	0.0050

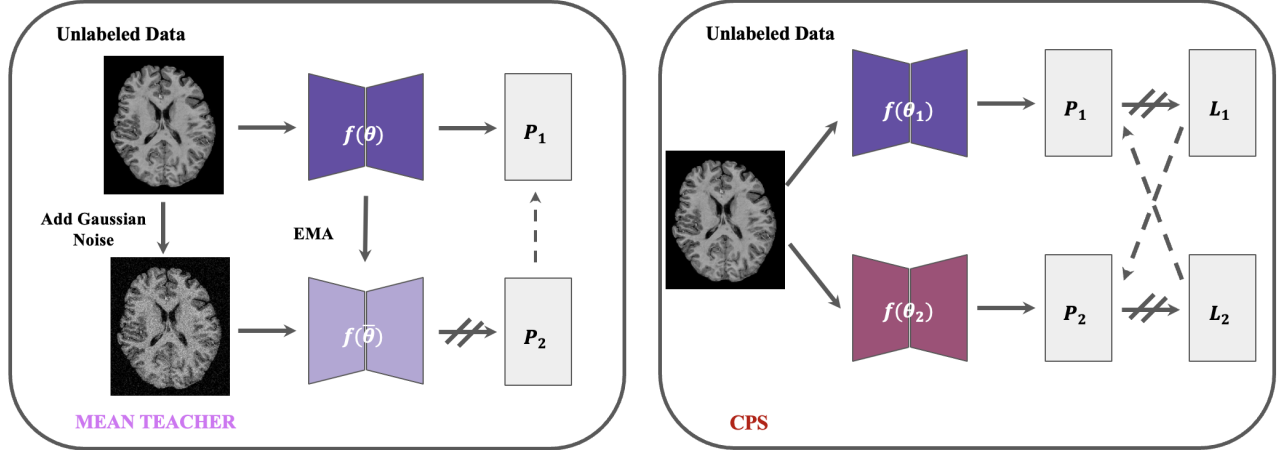


Figure 2. Illustration of the semi-supervised methods schema. The left panel shows the Mean Teacher model. The right panel shows the CPS model. ‘→’ means forward operations, ‘- ->’ means loss supervision, and ‘//’ means stop-gradient.

shown in the right panel of Figure 2. The two networks produce the probability outputs P_1 and P_2 , respectively. We apply argmax to these probability outputs to obtain one-hot labels, L_1 and L_2 . These labels are then used to supervise the training of the other branch, i.e., L_1 supervises P_2 , and L_2 supervises P_1 . The semi-supervised loss is calculated using $L_{unsup_1} = CE(L_2, P_1)$ and $L_{unsup_2} = CE(L_1, P_2)$. The network parameters $f(\theta_1)$ and $f(\theta_2)$ are updated using $L_{semi_1} = L_{sup_1} + \lambda_{semi} L_{unsup_1}$ and $L_{semi_2} = L_{sup_2} + \lambda_{semi} L_{unsup_2}$ respectively. We note that L_{sup_1} and L_{sup_2} are computed by passing labeled images into the networks $f(\theta_1)$ and $f(\theta_2)$, respectively.

2.4 Self-supervised training model in public 3T MRI datasets

In this section, we describe our self-supervised augmentation scheme for leveraging unlabeled 3T MRI datasets. We introduce random augmentations to our input images and use the pairs of real and augmented images for 3 proxy tasks to allow self-supervision, inspired by Tang et al.²⁵ To accomplish this, we concatenate three different task-specific heads after the encoder and compute three self-supervised losses: rotation prediction, inpainting reconstruction, and contrastive loss. The total self-supervised loss for the pre-training is defined as $L_{pre.training} = \lambda_1 L_{rot} + \lambda_2 L_{inpaint} + \lambda_3 L_{contrast}$ where λ_i are hyper-parameters. We choose $\lambda_1 = \lambda_2 = \lambda_3 = 1$ in our experiments.

2.4.1 Augmentation methods

Table 3 lists the three types of augmentation we apply and the associated parameters for each.

1. **Random rotations.** We follow the method of Chen et al.²⁶ and apply a combination of random rotations of $r \in \{0^\circ, 90^\circ, 180^\circ, 270^\circ\}$. The case $r = 180^\circ$ is illustrated in Figure 3 between panels $A \rightarrow B$.
2. **Random cutouts and patch swaps.** We choose random rectangular patches and replace it with either a different random patch in the brain or with random noise. Recall that the data is represented as sub-volumes of $96 \times 96 \times 96$ voxels in our models. The patch sizes are constrained to $[0.05, 0.25]$ of the sub-volume size along each dimension, and a total volume less than 30% of the sub-volume size. This augmentation is illustrated in Figure 3 between panels $A \rightarrow C$ and $B \rightarrow D$.
3. **Random histogram shifts.** We use the random histogram shift as implemented in MONAI (<https://monai.io>). This is illustrated in Figure 3 between panels $C \rightarrow E$ and $D \rightarrow F$. Note that we do not have a proxy task that leverages this augmentation; instead, the goal of this augmentation is to reduce the domain gap between 3T and 7T datasets by increasing the diversity of the training dataset.

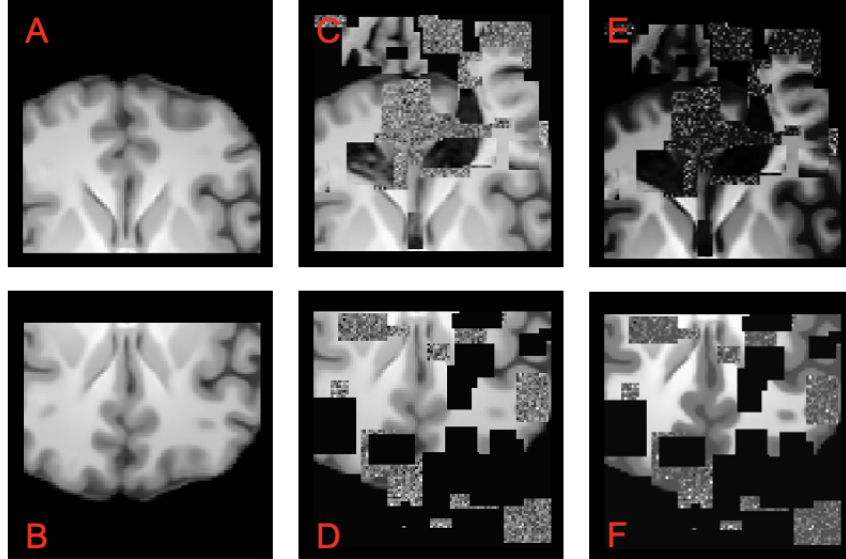


Figure 3. Augmentation for a subject from the UMCL dataset **A**. The cropped sub-volume of $96 \times 96 \times 96$. **A** \rightarrow **B**. Rotation of $r = 180^\circ$. **A** \rightarrow **C**, **B** \rightarrow **D**. Random cutout and patch swaps. **C** \rightarrow **E**, **D** \rightarrow **F**. Random histogram shifts.

2.4.2 Proxy Task 1: Rotation Prediction

The rotation prediction task is designed to ensure that the encoder learns to extract robust features that are invariant to rotation. We train the encoder to predict the rotation angle categories $r \in \{0^\circ, 90^\circ, 180^\circ, 270^\circ\}$ in the rotated sub-volume. A single multilayer perceptron (MLP) head is attached to the encoder to predict the softmax rotation angle possibilities \hat{P}_r given the ground truth P_r and cross-entropy loss is used for updating the parameters.

$$L_{rot} = - \sum_r^{0^\circ, 90^\circ, 180^\circ, 270^\circ} P_r \log(\hat{P}_r)$$

2.4.3 Proxy Task 2: Inpainting Reconstruction

The inpainting reconstruction task is designed to improve the encoder’s generalization ability and semantic understanding. We train the encoder to reconstruct the missing information from the random cutout and patch swaps. For the inpainting reconstruction, we apply a Variational Autoencoder (VAE)²⁷ head containing 6 3D convolution blocks with instance normalization. We add a leaky-ReLU activation on the downsampling path for each scale and an MLP layer on the upsampling path. Given the cutout patch I_{pred} and the original image I_{org} , we use the L1 Loss to train the reconstruction network.

$$L_{inpaint} = \|I_{pred} - I_{org}\|_1$$

2.4.4 Proxy Task 3: Contrastive Representation Learning

The contrastive representation learning task is designed to encourage the encoder to learn representations that are robust to different data augmentations and reduce the domain gap between different datasets. We create a minibatch of $2N$ samples by applying two random augmentations (combination of rotate/crop/histogram shift) to each of N subjects, such that the minibatch contains two views of each subject. Then, we randomly select two images from the minibatch and train the

Table 3. Data augmentation during our training process. **p** indicates the probability of applying an augmentation.

Transform	Parameters	p
Random Rotate	$r \in \{0^\circ, 90^\circ, 180^\circ, 270^\circ\}$	0.25, 0.25, 0.25, 0.25
Random Crop and Patch Swap	$v=0.3, b_{max} = 0.25, b_{min} = 0.05$	1
Random Histogram Shift	# control points = 1, 3	0.5, 0.5

encoder to predict whether they are from the same subject. Specifically, a linear MLP projection head is applied to map the latent features from the encoder into higher dimensions v . We use cosine-similarity²⁸ to maximize the agreement among positive pairs (same subject i , different augmentations) $v_{i,1}, v_{i,2}$ and minimize the negative pairs (different subjects i vs. k). Thus the loss function is defined as

$$L_{contrast} = -\log \frac{\exp(\text{sim}(v_{i,1}, v_{i,2})/t)}{\sum_{k=1, k \neq i}^N \sum_{j=1}^2 \exp(\text{sim}(v_{i,1}, v_{k,j})/t)},$$

where t is the temperature and $\text{sim}(\cdot)$ denotes cosine similarity.

2.5 Implementation Details

Given the input sub-volumes of size $96 \times 96 \times 96$, we use the Swin-Transformer window and patch size of $2 \times 2 \times 2$, which leads to $48 \times 48 \times 48$ patches. We use 4 down-sampling blocks and set the number of features to 12, resulting in a latent feature size of $(3 \times 3 \times 3) \times 2^4 \times 12$. We set the number of transformer heads as [3, 6, 12, 24]. For the pre-training stage, the contrastive head uses a latent feature vector v of size 512. The VAE reconstruction head uses a kernel size of 3 with 4 up-sampling stages. Our framework is implemented in PyTorch and MONAI on a single NVIDIA 2080Ti. The pre-training set is split into 80% for training and 20% for evaluation. We use the inpainting reconstruction L1 loss for our stopping criteria. For all semi-supervised strategies, we adopt $\lambda_{semi} = 1$ and used a stochastic gradient descent (SGD) with a learning rate of $lr = 1e^{-4}$.

3. RESULTS

3.1 Labeled training data size experiment

We first examine the performance of our model in the scenario of limited labeled data availability. This is a fairly common scenario in practice: for example, often, a new MRI protocol may need to be evaluated on a preliminary basis after the first few scans are acquired, before the entire dataset is collected. In this scenario, very few annotated images are available to train, but we can generally assume that unlabeled images from previous similar studies likely exist.

We split our labeled 7T in-house dataset (n=14) into 7 folds, with 12:2 train:test split in each fold. We evaluate three limited labeled dataset settings, using 3, 5 or 10 labeled images as training data. The remaining scans (12-3=9, 12-5=7, and 12-10=2, respectively) are treated as unlabeled data along with the unlabeled 7T in-house dataset (n=23).

We present the 7-fold average Dice similarity coefficients in Table 4. We observe that cross pseudo supervision (CPS) is again the best semi-supervised method and that it provides a dramatic performance increase (0.7915 vs. 0.6872 Dice) compared to the fully supervised model trained from scratch, i.e., on 7T data only. Even in the extreme scenario of only 3 training samples, our proposed framework can achieve comparable result to the fully supervised model with 10 training samples (0.6565 vs. 0.6872). We further observe that the 3T pre-training is beneficial to the 7T studies: the CPS with pre-training performs consistently better than CPS alone (e.g., 0.7541 vs. 0.7915 for 10 samples). These results are also presented in graphical format in Figure 4.

Table 4. Segmentation performance (Dice score) under varying amounts of labeled training data availability (Sec. 3.1). Bold text indicates the best performer and underlined text indicates the second best performer in each column.

Methods	Labeled training data size experiment		
	3 labeled samples	5 labeled samples	10 labeled samples
Fully supervised training on 7T only	0.5211±0.0227	0.6235±0.0107	0.6872±0.0358
Fully supervised training + Self-Supervised pre-train on 3T	0.5329±0.0196	0.6138±0.0400	0.6995±0.0154
Mean Teacher on 7T only	0.5734±0.0210	0.6173±0.0371	0.7109±0.0249
Cross Pseudo Supervision (CPS) on 7T only	0.6223±0.0321	0.6885±0.0206	0.7541±0.0126
Mean Teacher + Self-Supervised pre-train on 3T	0.6358±0.0203	0.6704±0.0184	0.7245±0.0193
CPS + Self-Supervised pre-train on 3T (SSL ²)	0.6565±0.0156	0.7345±0.0307	0.7915±0.0230

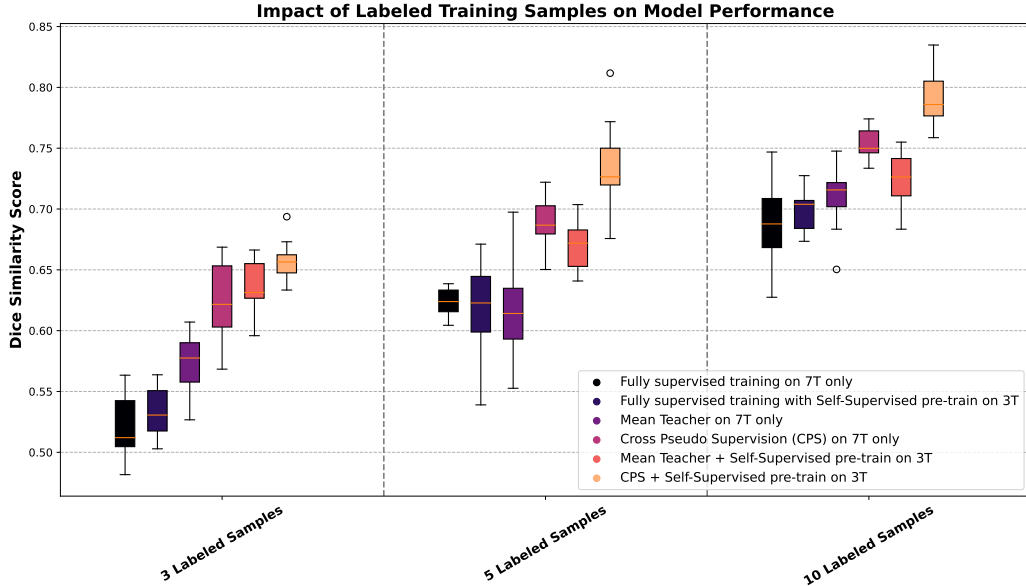


Figure 4. A box plot representation of the segmentation performance (Dice score) under varying amounts of labeled training data availability (Sec. 3.1). The brightest box is our proposed framework and has the best performance; the darkest box is the baseline model of fully supervised training from scratch.

3.2 Sparse labeling experiment

We next evaluate our model in a sparse labeling scenario. It can be challenging to carefully and confidently label all the images in an MRI scan due to constraints on time and effort. A potential solution can be to only label a subset of the 2D slices in a given 3D MRI volume. This can also be useful when some 2D slices are difficult to annotate due to poor image quality or artifacts. To examine the use of such sparse annotations, we vary the percentage of annotated slices in a given training image. The remaining slices and data from the unlabeled set are pooled together and used as the new unlabeled cohort for the experiment. For example, in the 20% setting, we randomly select 40 slices (200×0.20) as labeled data and use the remaining 160 as unlabeled data.

To allow a direct comparison to the experiments in Sec. 3.1, we randomly select 2 subjects for our test set and report the Dice score in Table 5. Similar to the training data size experiment, we note that CPS is the best performer. We observe that the self-supervised method contributes more than the semi-supervised method in this setting. We note that our proposed framework can outperform fully supervised training from scratch with 100% of the annotated data when using only 50% of annotations (0.7823 vs. 0.6971).

Finally, we present qualitative results in Figure 5. Our proposed framework (panel E) yields the closest results to the manual ground truth annotations. The results of the 7T fully supervised MRI showed comparable performance in some areas, but had many false negatives (especially in the top zoom panel), which can be problematic for clinical diagnosis. The self-supervised learning approach improved the detection in some of these regions, but our proposed method combining semi-supervised and self-supervised learning resulted in the best performance.

Table 5. Segmentation performance (Dice score) under varying amounts of sparsely labeled training data (Sec. 3.2). Bold text indicates the best performer and underlined text indicates the second best performer in each column.

Methods	Sparse labeling experiment			
	10 %	20 %	50 %	100 %
Fully supervised training on 7T only	0.5174	0.5732	0.6542	0.6971
Fully supervised training + Self-Supervised pre-train on 3T	0.6233	0.6422	0.6855	0.7121
Mean Teacher on 7T only	0.5673	0.5884	0.6627	0.7047
Cross Pseudo Supervision (CPS) on 7T only	0.6107	0.6342	0.7108	<u>0.7835</u>
Mean Teacher + Self-Supervised pre-train on 3T	<u>0.6411</u>	<u>0.6589</u>	<u>0.7232</u>	0.7624
CPS + Self-Supervised pre-train on 3T (SSL ²)	0.6523	0.6785	0.7823	0.8186

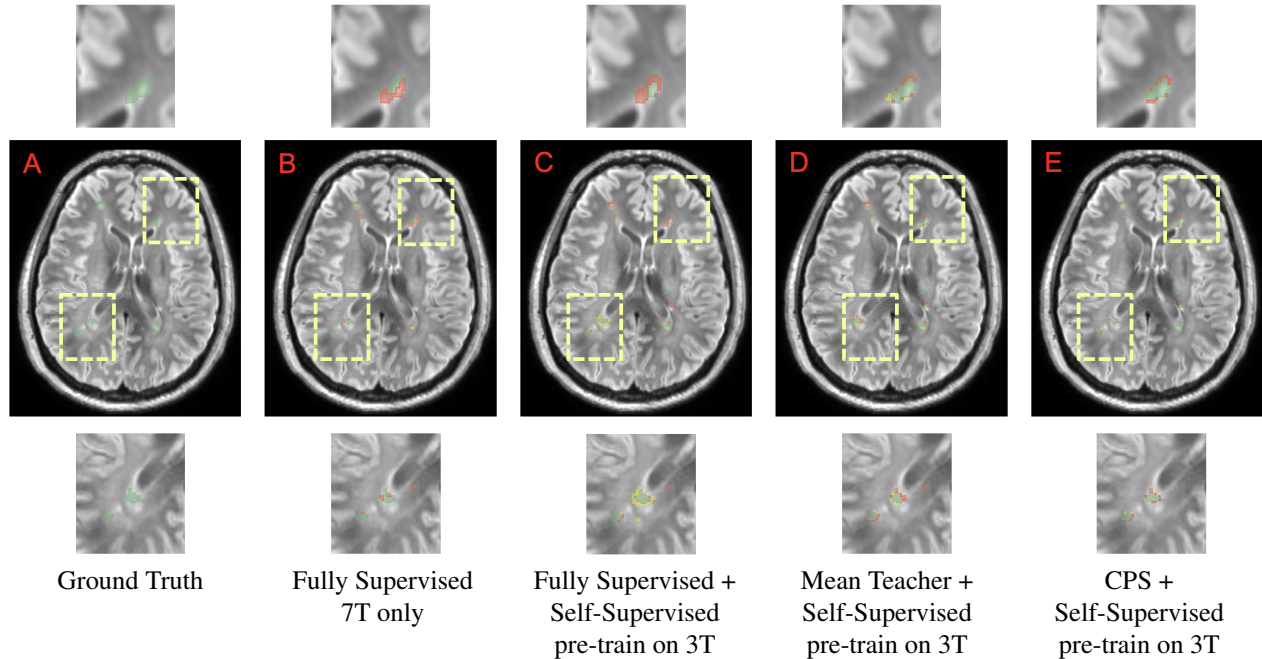


Figure 5. Qualitative segmentation results in our 7T dataset with 100% labeling and 12 labeled training samples. Segmentations are overlaid on the FLAIR image. Top and bottom rows show zoomed-in views of the yellow ROIs. Green denotes the true positives, red denotes false negatives, and yellow denotes false positives.

4. CONCLUSION

In this paper, we proposed a novel approach for achieving robust MS lesion segmentation in 7T brain MRI data by utilizing self-supervised training to embed information from publicly available 3T brain MRI data, in combination with semi-supervised techniques to leverage limited labeled 7T data. Our experimental results demonstrate the effectiveness of this approach, achieving higher accuracy with either a small number of training samples or sparsely annotated images.

We make the pre-trained weights of our proposed approach publicly available to benefit future 7T brain MRI studies. In future work, we aim to investigate the generalizability of our proposed pre-trained encoder to other 7T MRI studies as well as its potential for use in downstream tasks beyond lesion segmentation.

ACKNOWLEDGMENTS

This work was supported, in part, by NIH grant R01-NS094456 and National Multiple Sclerosis Society grant PP-1905-34001. Francesca Bagnato receives research support from Biogen Idec, the National Multiple Sclerosis Society (RG-1901-33190) and the National Institutes of Health (1R01NS109114-01). Francesca Bagnato did not receive financial support for the research, authorship and publication of this article.

REFERENCES

- [1] Liu, Z., Lin, Y., Cao, Y., Hu, H., Wei, Y., Zhang, Z., Lin, S., and Guo, B., “Swin Transformer: Hierarchical vision Transformer using shifted windows,” in *Proceedings of the IEEE/CVF International Conference on Computer Vision*, 10012–10022 (2021).
- [2] Roy, S., Butman, J. A., Reich, D. S., Calabresi, P. A., and Pham, D. L., “Multiple Sclerosis lesion segmentation from brain MRI via fully convolutional neural networks,” *arXiv preprint arXiv:1803.09172* (2018).
- [3] Danelakis, A., Theoharis, T., and Verganelakis, D. A., “Survey of automated Multiple Sclerosis lesion segmentation techniques on Magnetic Resonance Imaging,” *Computerized Medical Imaging and Graphics* **70**, 83–100 (2018).
- [4] Zhang, H., Valcarcel, A. M., Bakshi, R., Chu, R., Bagnato, F., Shinohara, R. T., Hett, K., and Oguz, I., “Multiple Sclerosis lesion segmentation with Tiramisu and 2.5 d stacked slices,” in *International Conference on Medical Image Computing and Computer-Assisted Intervention*, 338–346, Springer (2019).

- [5] Zhang, H., Li, H., and Oguz, I., “Segmentation of new ms lesions with tiramisu and 2.5 d stacked slices,” *MSSEG-2 challenge proceedings: Multiple sclerosis new lesions segmentation challenge using a data management and processing infrastructure*, 61 (2021).
- [6] Liu, H., Fan, Y., Li, H., Wang, J., Hu, D., Cui, C., Lee, H. H., and Oguz, I., “ModDrop++: A dynamic filter network with intra-subject co-training for Multiple Sclerosis lesion segmentation with missing modalities,” *arXiv preprint arXiv:2203.04959* (2022).
- [7] Taleb, A., Loetzsch, W., Danz, N., Severin, J., Gaertner, T., Bergner, B., and Lippert, C., “3D self-supervised methods for medical imaging,” *Advances in Neural Information Processing Systems* **33**, 18158–18172 (2020).
- [8] Cheplygina, V., de Bruijne, M., and Pluim, J. P., “Not-so-supervised: a survey of semi-supervised, multi-instance, and transfer learning in medical image analysis,” *Medical image analysis* **54**, 280–296 (2019).
- [9] Tarvainen, A. and Valpola, H., “Mean teachers are better role models: Weight-averaged consistency targets improve semi-supervised deep learning results,” *Advances in neural information processing systems* **30** (2017).
- [10] Chen, X., Yuan, Y., Zeng, G., and Wang, J., “Semi-supervised semantic segmentation with cross pseudo supervision,” in *[Proceedings of the IEEE/CVF Conference on Computer Vision and Pattern Recognition]*, 2613–2622 (2021).
- [11] Hatamizadeh, A., Tang, Y., Nath, V., Yang, D., Myronenko, A., Landman, B., Roth, H. R., and Xu, D., “Unetr: Transformers for 3D medical image segmentation,” in *[Proceedings of the IEEE/CVF Winter Conference on Applications of Computer Vision]*, 574–584 (2022).
- [12] Li, H., Hu, D., Liu, H., Wang, J., and Oguz, I., “Cats: Complementary CNN and Transformer encoders for segmentation,” in *[2022 IEEE 19th International Symposium on Biomedical Imaging (ISBI)]*, 1–5, IEEE (2022).
- [13] Hatamizadeh, A., Nath, V., Tang, Y., Yang, D., Roth, H. R., and Xu, D., “Swin Unetr: Swin Transformers for semantic segmentation of brain tumors in MRI images,” in *[International MICCAI Brainlesion Workshop]*, 272–284, Springer (2022).
- [14] Carass, A., Roy, S., Jog, A., Cuzzocreo, J. L., Magrath, E., Gherman, A., Button, J., Nguyen, J., Prados, F., Sudre, C. H., et al., “Longitudinal Multiple Sclerosis lesion segmentation: resource and challenge,” *NeuroImage* **148**, 77–102 (2017).
- [15] Lesjak, Ž., Galimzianova, A., Koren, A., Lukin, M., Pernuš, F., Likar, B., and Špiclin, Ž., “A novel public MR image dataset of Multiple Sclerosis patients with lesion segmentations based on multi-rater consensus,” *Neuroinformatics* **16**(1), 51–63 (2018).
- [16] Commowick, O., Cervenansky, F., and Ameli, R., “Msseg challenge proceedings: Multiple Sclerosis lesions segmentation challenge using a data management and processing infrastructure,” in *[Miccai]*, (2016).
- [17] Menze, B. H., Jakab, A., Bauer, S., Kalpathy-Cramer, J., Farahani, K., Kirby, J., Burren, Y., Porz, N., Slotboom, J., Wiest, R., et al., “The multimodal brain tumor image segmentation benchmark (BRATS),” *IEEE transactions on medical imaging* **34**(10), 1993–2024 (2014).
- [18] Isensee, F., Schell, M., Pflueger, I., Brugnara, G., Bonekamp, D., Neuberger, U., Wick, A., Schlemmer, H.-P., Heiland, S., Wick, W., et al., “Automated brain extraction of multisequence MRI using artificial neural networks,” *Human brain mapping* **40**(17), 4952–4964 (2019).
- [19] Tustison, N. J., Avants, B. B., Cook, P. A., Zheng, Y., Egan, A., Yushkevich, P. A., and Gee, J. C., “N4ITK: improved n3 bias correction,” *IEEE transactions on medical imaging* **29**(6), 1310–1320 (2010).
- [20] Vu, T.-H., Jain, H., Bucher, M., Cord, M., and Pérez, P., “Advent: Adversarial entropy minimization for domain adaptation in semantic segmentation,” in *[Proceedings of the IEEE/CVF Conference on Computer Vision and Pattern Recognition]*, 2517–2526 (2019).
- [21] Zhang, Y., Yang, L., Chen, J., Fredericksen, M., Hughes, D. P., and Chen, D. Z., “Deep adversarial networks for biomedical image segmentation utilizing unannotated images,” in *[International conference on medical image computing and computer-assisted intervention]*, 408–416, Springer (2017).
- [22] Yu, L., Wang, S., Li, X., Fu, C.-W., and Heng, P.-A., “Uncertainty-aware self-ensembling model for semi-supervised 3D left atrium segmentation,” in *[International Conference on Medical Image Computing and Computer-Assisted Intervention]*, 605–613, Springer (2019).
- [23] Sohn, K., Berthelot, D., Carlini, N., Zhang, Z., Zhang, H., Raffel, C. A., Cubuk, E. D., Kurakin, A., and Li, C.-L., “Fixmatch: Simplifying semi-supervised learning with consistency and confidence,” *Advances in neural information processing systems* **33**, 596–608 (2020).
- [24] Luo, X., Wang, G., Liao, W., Chen, J., Song, T., Chen, Y., Zhang, S., Metaxas, D. N., and Zhang, S., “Semi-supervised medical image segmentation via uncertainty rectified pyramid consistency,” *Medical Image Analysis* **80**, 102517 (2022).

- [25] Tang, Y., Yang, D., Li, W., Roth, H. R., Landman, B., Xu, D., Nath, V., and Hatamizadeh, A., “Self-supervised pre-training of Swin Transformers for 3D medical image analysis,” in [*Proceedings of the IEEE/CVF Conference on Computer Vision and Pattern Recognition*], 20730–20740 (2022).
- [26] Chen, L., Bentley, P., Mori, K., Misawa, K., Fujiwara, M., and Rueckert, D., “Self-supervised learning for medical image analysis using image context restoration,” *Medical image analysis* **58**, 101539 (2019).
- [27] An, J. and Cho, S., “Variational autoencoder based anomaly detection using reconstruction probability,” *Special Lecture on IE* **2**(1), 1–18 (2015).
- [28] Chen, X., Fan, H., Girshick, R., and He, K., “Improved baselines with momentum contrastive learning,” *arXiv preprint arXiv:2003.04297* (2020).